

UCLA

UCLA Electronic Theses and Dissertations

Title

Modeling and Performance of Pyroelectric Detector Lithium Niobate under Ringing Signal Suppression

Permalink

<https://escholarship.org/uc/item/1jb0868s>

Author

Peng, Gary Meng Kiang

Publication Date

2013

Peer reviewed|Thesis/dissertation

UNIVERSITY OF CALIFORNIA

Los Angeles

Modeling and Performance of Pyroelectric Detector Lithium Niobate under Ringing
Signal Suppression

A thesis submitted in partial satisfaction of the requirements for the degree

Master of Science in

Electrical Engineering

By

Gary Meng Kiang Peng

2013

© Copyright by

Gary Meng Kiang Peng

2013

ABSTRACT OF THE THESIS

Modeling and Performance of Pyroelectric Detector Lithium Niobate Under Ringing Signal Suppression

By

Gary Meng Kiang Peng

Master of Science in Electrical Engineering

University of California, Los Angeles, 2013

Professor Oscar Stafsudd, Chair

Lithium Niobate (LiNbO_3) is an excellent photo sensor that can be used in medical imaging, weapons guidance systems, radiation detection, and many other light sensitive applications. It can operate at its natural state without requiring extensive heating or cooling modifications. However, when LiNbO_3 is used as a photo detector, its functionality becomes limited because it produces many signal oscillations. These oscillations make the real signal and the background noise indistinguishable. This phenomenon is known as the “Ringing Effect.” To address this issue, Lithium Niobate is cut at a crystal orientation that reduces signal oscillations. In this paper I present: the experimental set up, device performance, along with detailed derivations of the circuit model, temperature, and charge models that are specific to LiNbO_3 .

Ringing suppressions were tested under three sets of variables: 1) various sample thicknesses; 2) different irradiation angles; 3) the addition of a black absorbing layer on the

illuminated surface. The resulting signal response time under the previously mentioned circumstances were measured and compared.

Our conclusion is that ringing effect can be reduced by a correct crystal cut. The attained signal response time under ringing suppression was in the sub-nanosecond range. The added black coating layer on the illuminated surface did not always give faster performance. It was observed that a decrease in the sample thickness could reduce response time.

The thesis of Gary Meng Kiang Peng is approved.

Jia Ming Liu

Warren Grundfest

Oscar Stafsudd, Committee Chair

University of California, Los Angeles

2013

Table of Contents

ABSTRACT OF THE THESIS	ii
Table of Contents	v
Index of symbols and constants	vii
List of Tables	viii
List of Figures	ix
CHAPTER 1 INTRODUCTION	1
CHAPTER 2 DEVICE MODEL AND SET UP	3
2.1 Device Configuration	3
2.2 Device Electrical Equivalent Circuit	4
2.3 Noise Sources	5
1) Johnson Noise	5
2) Amplifier Noise	5
3.1 Absorptivity and Radiation of Black Bodies	6
3.2 Linear Heat Conduction for the Sinusoidal Modulated Heat Flow	7
Case 1 : Thin layers or low frequencies (ωb small) :	11
Case 2: ωb is much smaller than one, and $\frac{K\omega}{H}$ is much larger than one:	11
Case 3: Thick layer or high frequencies (ωb large) :	12
3.3 Charge Model	12
3.4 Total Energy Laser Detector	15
CHAPTER 4 SAMPLES AND EXPERIMENT	19

CHAPTER 5 RESULTS AND DISCUSSION.....	20
5.1 Not-Coated Samples under N ₂ Laser Exposure	21
5.2 Black Coated Samples under N ₂ Laser Exposure	26
5.3 Modulated Diode Laser as the Light Source.....	30
CHAPTER 6 SUMMARY AND CONCLUSION	35
Appendix A – Temperature Profile When T _{back} ≠ 0	36
Appendix B – Temperature Only Varies With Distance <i>x</i>	38
References.....	40

Index of symbols and constants

Symbol	Definition	Unit
α	Absorptivity (fraction absorbed)	[unit less]
$\rho_{reflectivity}$	Reflectivity (fraction reflected)	[unit less]
ε	Emissivity	[unit less]
q	Heat flow	[W]
A	Body surface area	[m ²]
σ	Stephan constant = 5.676×10^{-8}	$\left[\frac{W}{m^2 \cdot K^4} \right]$
T, θ	Temperature	[K]
H	Radiation conductance or radiated heat transfer coefficient	$\left[\frac{W}{K} \right]$
K	Thermal Conductivity	$\left[\frac{W}{cm \cdot K} \right]$

List of Tables

Table 3.4-1 Lithium Niobate LiNbO ₃ thermal properties at 300K.	15
Table 3.4-2 Calculated limits of the detector size and the light exposure time.	16
Table 5.1-1 Response time summary for the not-coated samples under N ₂ laser exposure.	24
Table 5.2-1 Response time summary for the black-coated samples under N ₂ laser exposure.	28
Table 5.3 -1 Response time summary for samples under diode laser exposure.	33

List Of Figures

<i>Figure 2.1- 1 Face-Electrode Configuration.....</i>	<i>3</i>
<i>Figure 2.1- 2 Edge-Electrode Configuration.....</i>	<i>3</i>
<i>Figure 2.2- 1 General electrical circuit for the detector and the amplifier input.</i>	<i>4</i>
<i>Figure 2.2- 2 Simplified detector electrical equivalent circuit.</i>	<i>5</i>
<i>Figure 3.2- 1 Single layer pyroelectric detector with radiation from the back surface.</i>	<i>9</i>
<i>Figure 3.3- 1 Edge-Electrode Configuration.....</i>	<i>13</i>
<i>Figure 4.1- 1 Experiment Schematic Set Up.....</i>	<i>19</i>
<i>Figure 5.0 - 1 Signal response between ringing suppressed and not-suppressed samples</i>	<i>20</i>
<i>Figure 5.1- 1 Not-coated, 0.5 mm thick, N₂ laser frontal exposure response.</i>	<i>22</i>
<i>Figure 5.1- 2 Not-coated, 1.5 mm thick, N₂ laser frontal exposure response.</i>	<i>22</i>
<i>Figure 5.1- 3 Not-coated, 2.5 mm thick, N₂ laser frontal exposure response.</i>	<i>23</i>
<i>Figure 5.1- 4 Not-coated, 4.0 mm thick, N₂ laser frontal exposure response.</i>	<i>23</i>
<i>Figure 5.1- 5 Not-coated, 1.5 mm thick, N₂ laser side exposure response.</i>	<i>24</i>
<i>Figure 5.1- 6 Not-coated, 2.5 mm thick, N₂ laser side exposure response.</i>	<i>24</i>
<i>Figure 5.1- 7 Full response time comparison between the frontal and the side exposure under N₂ laser.....</i>	<i>25</i>
<i>Figure 5.2- 1 Black-coated, 0.5 mm thick, N₂ laser frontal exposure response.</i>	<i>26</i>
<i>Figure 5.2- 2 Black-coated, 1.5 mm thick, N₂ laser frontal exposure response.</i>	<i>27</i>
<i>Figure 5.2- 3 Black-coated, 2.5 mm thick, N₂ laser frontal exposure response.</i>	<i>27</i>
<i>Figure 5.2- 4 Black-coated, 4.0 mm thick, N₂ laser frontal exposure response.</i>	<i>28</i>

<i>Figure 5.2- 5 Full response time comparison between Black-coated and Not-Coated samples under N₂ laser exposure</i>	<i>28</i>
<i>Figure 5.3 - 1 Not-coated, 0.5 mm thick, Diode laser frontal exposure response.....</i>	<i>30</i>
<i>Figure 5.3 - 2 Not-coated, 1.5 mm thick, diode laser frontal exposure response.....</i>	<i>31</i>
<i>Figure 5.3 - 3 Not-coated, 2.5mm thick, diode laser frontal exposure response.....</i>	<i>31</i>
<i>Figure 5.3 - 4 Not-coated, 4.0 mm thick, diode laser frontal exposure response.....</i>	<i>32</i>
<i>Figure 5.3 – 5 Black-coated, 2.5mm thick, diode laser frontal exposure response.....</i>	<i>32</i>
<i>Figure 5.3 – 6 Black-coated, 4mm thick, diode laser frontal exposure response.....</i>	<i>33</i>
<i>Figure 5.3 – 7 Not-coated and black-coated sample response time comparison under diode laser exposure.</i>	<i>33</i>
<i>Figure A - 1 Single layer pyroelectric detector with radiation from back surface.....</i>	<i>36</i>
<i>Figure B - 1 Temperature that only varies in x in a detector</i>	<i>38</i>

CHAPTER 1 INTRODUCTION

Lithium Niobate (LiNbO_3) is an insulator and is considered a piezoelectric base in its crystal structure. It is also a pyroelectric because temperature variation can change its dipole moment. Pyroelectrics are light sensors and can be used in medical imaging, radiation monitors, weapons guidance systems, and many other photon sensitive applications. It is crucial to note that solid state crystals are not the only class of materials that can exhibit the pyroelectric effect, Polyvinylidene fluoride film also has been demonstrated to have pyroelectric properties [1]. Although each application has its own set of device selection criteria, one common interest is to have natural state operation, especially at room temperature. LiNbO_3 is an excellent candidate to satisfy this need. It can function at its natural state without requiring extensive heating or cooling modifications besides what are present in the ambient environment; therefore, it is more portable and cost advantageous.

The major advantage of using Lithium Niobate over the traditional semiconductor photo detector is the impact of its wide band gap on intrinsic carriers. The material band gap determines the intrinsic carrier population inside the semiconductor at a given temperature. The higher the band gap, the smaller the intrinsic carrier population [2]. Since the intrinsic carriers act as background noise and set the minimum detectable signal amplitude, a low intrinsic carrier population is typically desired. The band gap is an inherent material property and cannot be easily changed, whereas the temperature can be externally controlled to alter the carrier concentration. In practice, an external cooling apparatus is applied onto the detector to reduce background noise, especially in narrow band gap photo sensors. The added cooling component can become problematic in weight sensitive applications like missiles. But LiNbO_3 is an

insulator with a wide band gap. It naturally has low carrier concentration; hence, no extra cooling is needed.

However, LiNbO_3 is not free from issues. Because it is a piezoelectric, any applied electric field will create strain on the crystal; the mounting of clamps or electrodes on the crystal will generate stress. Stress and strain will change the crystal electric polarization. The change in the crystal electric polarization as a result of temperature change, applied electric field, and mechanical stress, produces oscillations in detector response signals [3]. This signal oscillation is known as the “Ringing Effect.” The Ringing Effect prolongs the decay time of the detector’s excited signal response, and will thus limit the detector’s operating range at the high frequency mode. For example, when the first signal fails to decay, it will become noise and add to the incoming second signal. There will be no indication to tell where does one signal end and another signal begin. To counter this problem, LiNbO_3 crystal is cut at an orientation that dampens signal oscillations, and the resulting device performance is investigated.

CHAPTER 2 DEVICE MODEL AND SET UP

2.1 Device Configuration

There are two ways to configure a pyroelectric detector by changing the electrode placement on the detector. The Face-Electrode arrangement shown in Figure 2.1-1 has electrodes on the surfaces that face the incoming radiation.

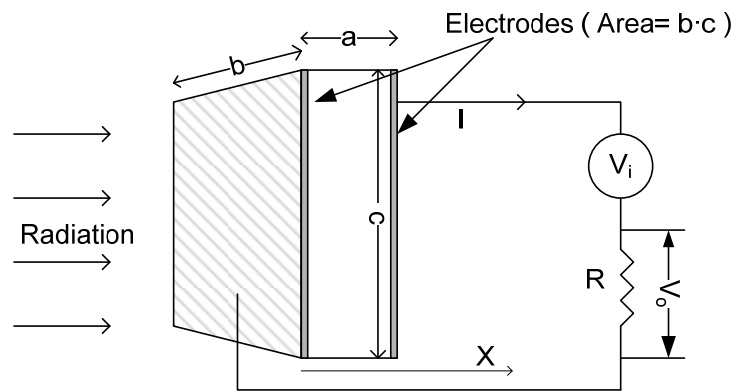


Figure 2.1- 1 Face-Electrode Configuration.

The Edge-Electrode configuration shown in Figure 2.1.2 has electrodes at the edge surfaces that are parallel to the radiation direction.

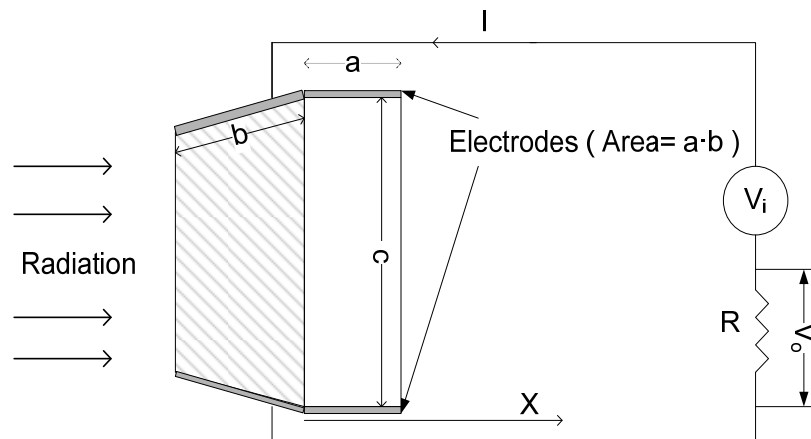


Figure 2.1- 2 Edge-Electrode Configuration.

One of the advantages that the Edge-Electrode has over the Face-Electrode configuration is the internal electric capacitance C_D ,

$$C_D = \frac{\epsilon_o \epsilon_D}{t} \cdot Area \quad (2.1.1)$$

For the Edge-Electrode configuration, $t = c$; it is constant. For the Face-Electrode configuration, $t = a$, t varies with device thickness in the direction of x . As a decreases, the capacitance C_D will increase, and the RC time delay will also increase. In addition, the Edge-Electrode configuration has a smaller electrode area than the Face-Electrode configuration.

2.2 Device Electrical Equivalent Circuit

According to Putley [4], the general electrical circuit of the detector and the amplifier input is given by Figure 2.2-1.

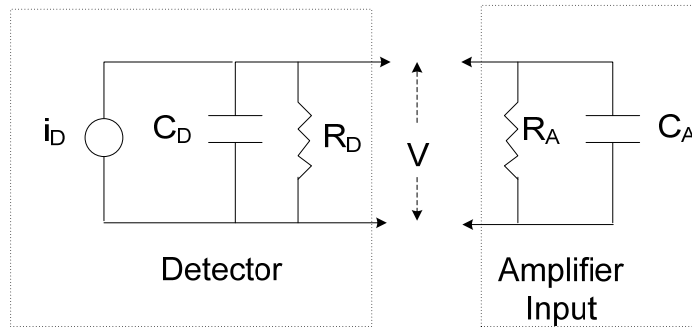


Figure 2.2- 1 General electrical circuit for the detector and the amplifier input.

Since Lithium Niobate (LiNbO_3) is an insulator, its resistance R_D is large and can be treated as an open circuit. Figure 2.2-2 shows the simplified detector electrical circuit,

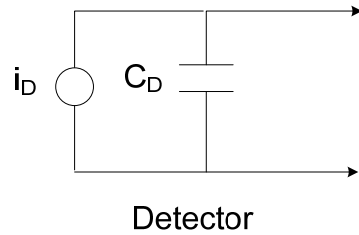


Figure 2.2- 2 Simplified detector electrical equivalent circuit.

2.3 Noise Sources

Base on Figure 2.2-1 and Figure 2.2-2, there are some qualitative conclusions on noise sources that can be drawn.

1) Johnson Noise

Because Johnson noise is related to resistance R , Johnson noise from LiNbO_3 's R_D will be *insignificant* when compared to R_A from the amplifier. The reason lies in the parallel resistor configurations as shown in Figure 2.2-1 and Figure 2.2-2. When $R_D \parallel R_A$ and $R_D \gg R_A$, the effective resistance is simply controlled by R_A , and so is the Johnson noise that comes with it.

2) Amplifier Noise

The equivalent circuit in Figure 2.2-1 shows two noise generators R_A and C_A from the amplifier. The noise generated by R_A and C_A will be compounded into the amplified voltage V . Therefore, it is expected that the amplifier will be the dominating noise contributor in the whole set up.

CHAPTER 3 THEORY

3.1 Absorptivity and Radiation of Black Bodies

When thermal radiation falls upon an object, a part of the radiation is absorbed by the body, the other part is reflected back into space. For a body that is opaque to the radiation transmission,

$$\alpha + \rho_{\text{reflectivity}} = 1.0 \quad (3.1.1)$$

where α is absorptivity (fraction absorbed) and $\rho_{\text{reflectivity}}$ is reflectivity (fraction reflected).

A *black body* is defined as one that absorbs all the radiant energy and reflects none. Hence, $\rho_{\text{reflectivity}} = 0$ and $\alpha = 1.0$ for a black body. Depending on its temperature, a black body also emits radiation. The ratio of an object surface's emissive power to that of a black body is *emissivity* e and it is 1.0 for a black body. For any black or non-black solid surface, Kirchhoff's law states that at the same temperature T , absorptivity and emissivity of a given surface are the same,

$$\alpha = e \quad (3.1.2)$$

The heat radiation from a body can be modeled by Stefan's Law,

$$q = A \cdot e \cdot \sigma \cdot T^4 \quad (3.1.3)$$

where q = heat flow [W] , e = emissivity

$$A = \text{body surface area [m}^2 \text{]}, \quad \sigma = 5.676 \times 10^{-8} \left[\frac{\text{W}}{\text{m}^2 \cdot \text{K}^4} \right],$$

T = temperature of the black body [K]

For an object with area A_1 at temperature T_1 place in an environment that is at temperature T_2 , the net heat radiation from the body to the surrounding will simply be,

$$\text{Net Heat} = \begin{array}{l} \text{Heat radiated} \\ \text{by body} \end{array} - \begin{array}{l} \text{Heat absorbed by body} \\ \text{from environment} \end{array} \quad (3.1.4)$$

Therefore, if the object is a perfect black body and the environment produces negligible radiation, i.e., $e_1 = \alpha_{12}$,

$$q_{net} = A_1 e_1 \sigma T_1^4 - A_1 \alpha_{12} \sigma T_2^4 = A_1 \cdot e_1 \cdot \sigma \cdot (T_1^4 - T_2^4) \quad (3.1.5)$$

where α_{12} is the absorptivity of body 1 for the radiation from the environment at T_2 .

Assume the environment temperature T_2 is constant, taking the derivative of Eqn. (3.1.5) gives the radiation conductance H , or also known as radiated heat transfer coefficient,

$$H = \frac{\partial q_{net}}{\partial T} = 4Ae_1\sigma T_1^3 \quad (3.1.6)$$

This heat transfer coefficient tells how well the energy can be transferred between the two mediums and it will be used to model heat flow inside the detector.

3.2 Linear Heat Conduction for the Sinusoidal Modulated Heat Flow

It is important to know how heat spreads inside the detector to build the heat flow model. Heat does not always spread uniformly in all dimensions. Heat flow direction can be restricted either by material property or physical dimension limitations. If the transient radiation is absorbed onto a surface and conducted as heat into the pyroelectric detector, the problem can be described as *one dimensional* heat flow. Base on the method described by Holman (1972) [5],

the time dependent temperature profile of a freely suspended pyroelectric detector under modulated radiations is derived. However, this method is only valid for small temperature excursions.

The one dimensional heat flow equation is

$$\frac{\partial \theta}{\partial t} = \kappa \frac{\partial^2 \theta}{\partial x^2} \quad (3.2.1)$$

and

$$\kappa = \frac{K}{\rho \cdot c} \quad (3.2.2)$$

where θ = temperature t = time
 κ = thermal diffusivity x = distance
 K = thermal conductivity ρ = density
 c = specific heat

The general solution to Equation (3.2.1) has time varying and time independent parts,

$$\theta = \theta_0 + T(x) \exp(j\omega_0 t) \quad (3.2.3)$$

where ω_0 is the angular frequency of the modulated heat flow.

$$T(x) = A \cosh(\omega x) + B \sinh(\omega x) \quad (3.2.4)$$

and

$$\omega = \left(\frac{j\omega_0}{\kappa} \right)^{\frac{1}{2}} = (1+j) \left(\frac{\omega_0}{2\kappa} \right)^{\frac{1}{2}} \quad (3.2.5)$$

θ_0 is time independent and it varies in distance x only. Its actual term is derived in Appendix B.

Figure 3.2-1 depicts the mathematical setup diagram for a freely suspended pyroelectric detector.

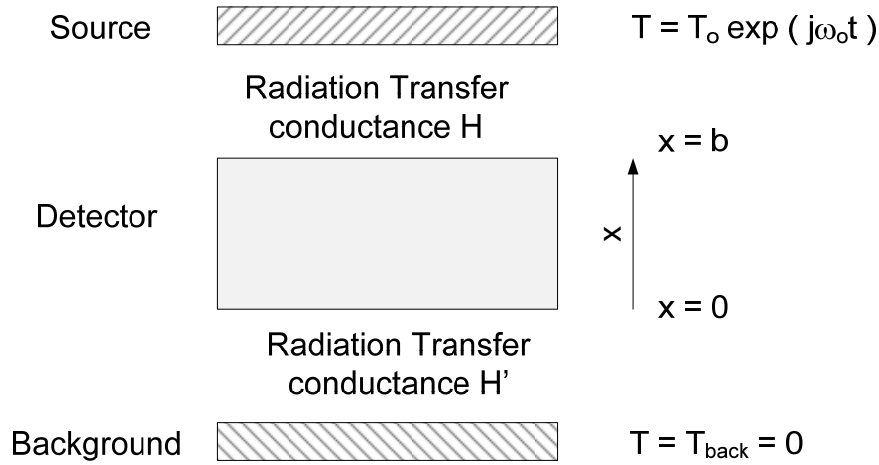


Figure 3.2- 1 Single layer pyroelectric detector with radiation from the back surface.

The background temperature is the reference point and it is set to zero for mathematic simplicity.

Appendix A will show the modification term if $T_{back} \neq 0$

The one dimensional Fourier's law of heat conduction is

$$\frac{q_x}{A} = -K \frac{\partial T}{\partial x} \quad (3.2.6)$$

where q_x is the heat transfer rate in the x direction, A is the cross sectional area.

The boundary conditions are:

- (1) At the contact boundary between the two medias, the heat conductivity is continuous

$$K_1 \frac{\partial T_1}{\partial x} = K_2 \frac{\partial T_2}{\partial x} \quad (3.2.7)$$

- (2) At the surface contact, the temperature is continuous

$$T_1 = T_2 \quad (3.2.8)$$

- (3) At the radiation exchanging surface with time varying components

$$K \frac{\partial T}{\partial x} = H (T_o - T) \quad (3.2.9)$$

Base on Fig. 3.2-1, start from Equation (3.2.4),

$$T(x) = A \cosh(\omega x) + B \sinh(\omega x) \quad (3.2.10)$$

$$\frac{\partial T}{\partial x} = A\omega \sinh(\omega x) + \omega B \cosh(\omega x)$$

At $x = 0$, assume $T_{back} = 0$

$$K \frac{\partial T}{\partial x} = H'(T - T_{back}) = H'T \quad (3.2.11)$$

and get

$$B = \frac{H'}{K\omega} A \quad (3.2.12)$$

At $x = b$,

$$K \frac{\partial T}{\partial x} = H(T_o - T) \quad (3.2.13)$$

$$K\omega[A \sinh(\omega b) + B \cosh(\omega b)] = H[T_o - A \cosh(\omega b) - B \sinh(\omega b)]$$

Substitute B from Equation (3.2.12) and solve for coefficient A

$$A = \frac{T_o}{\left(\frac{K\omega}{H} + \frac{H'}{K\omega}\right) \sinh(\omega b) + \left(\frac{H'}{H} + 1\right) \cosh(\omega b)} \quad (3.2.14)$$

Solving with these boundary conditions yields,

$$\begin{aligned} T(x) &= A \cosh(\omega x) + B \sinh(\omega x) \\ &= A \cosh(\omega x) + \frac{H'}{K\omega} A \sinh(\omega x) \end{aligned}$$

$$T(x) = \frac{\left[\cosh(\omega x) + \left(\frac{H'}{K\omega}\right) \sinh(\omega x) \right]}{\left[\left(\frac{K\omega}{H}\right) + \left(\frac{H'}{K\omega}\right) \right] \sinh(\omega b) + \left[\frac{H'}{H} + 1 \right] \cosh(\omega b)} \cdot T_o \quad (3.2.14)$$

The average layer temperature T_m is

$$T_m = \frac{1}{b \int_0^b T \cdot dx} \quad (3.2.15)$$

Substitute Equation (3.2.14) into Equation (3.2.15) yields

$$T_m = \frac{\left[\sinh(\omega b) + \left(\frac{H'}{K\omega} \right) (\cosh(\omega b) - 1) \right]}{\left[\left(\frac{K\omega}{H} \right) + \left(\frac{H'}{K\omega} \right) \right] \sinh(\omega b) + \left[\frac{H'}{H} + 1 \right] \cosh(\omega b)} \cdot \left(\frac{T_0}{\omega b} \right) \quad (3.2.16)$$

At first glance, Equation (3.2.14) and (3.2.16) are long and the dominating factors are difficult to find from within. From a design perspective, it is beneficial to know how the model will behave under different hypothetical operating circumstances.

There are several limiting cases can simplify Equation (3.2.14) and (3.2.16).

Case 1 : Thin layers or low frequencies (ωb small):

$$T(x) = T_m = \frac{T_0}{\left[\left(\frac{H'}{H} \right) + 1 \right]} \quad (3.2.17)$$

Equation (3.2.17) is applicable in scenarios like using low frequency light source or shrinking the device to increase compactness in a space restricted environment. In this case where ωb is small, temperature no longer varies with thickness but becomes uniform throughout the sample.

Case 2: ωb is much smaller than one, and $\frac{K\omega}{H}$ is much larger than one:

$$T(x) = T_m = \frac{HT_0}{K\omega^2 b} \quad (3.2.18)$$

Case 3: Thick layer or high frequencies (ωb large):

This estimate can be used in high frequency laser applications. Another situation to apply this simplification is when a device needs to be kept thick either because of its fragility or when there is limited wafer thinning capability.

Using Hyperbolic function properties

$$\sinh(x) = \frac{1}{2}(e^x - e^{-x}) \xrightarrow{\lim x \rightarrow \infty} \frac{1}{2}e^x \xrightarrow{x=\omega b} \frac{1}{2}e^{\omega b}$$

$$\cosh(x) = \frac{1}{2}(e^x + e^{-x}) \xrightarrow{\lim x \rightarrow \infty} \frac{1}{2}e^x \xrightarrow{x=\omega b} \frac{1}{2}e^{\omega b}$$

yield

$$T(x) = \frac{2 \exp(-\omega b) \left[\cosh(\omega x) + \left(\frac{H'}{K\omega} \right) \sinh(\omega x) \right]}{\left[1 + \left(\frac{H'}{K\omega} \right) \right] \left[1 + \left(\frac{K\omega}{H} \right) \right]} \cdot T_0 \quad (3.2.19)$$

The average layer temperature becomes

$$T_m = \frac{T_0}{\left[1 + \left(\frac{K\omega}{H} \right) \right] \omega b} \quad (3.2.20)$$

The temperature profile of the detector is now defined. The next logical step is to find its electrical correlation so it can be measured electronically.

3.3 Charge Model

The goal of pyroelectric application is to absorb heat, and then change pyroelectric material's polarization to produce charges. These charges are extracted through electrodes and

are measured through the electronic equipment. To keep track of these charges, the model uses the Edge-Electrode as the base configuration,

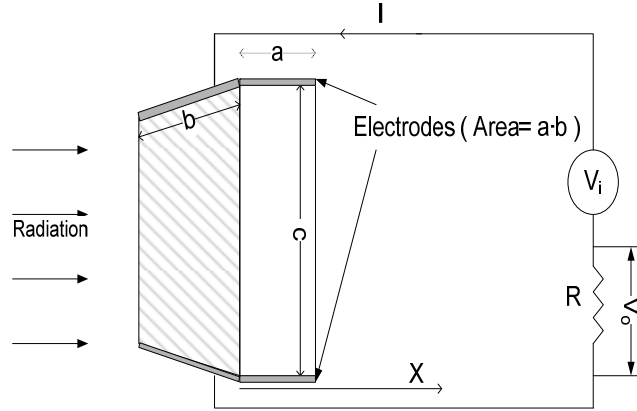


Figure 3.3- 1 Edge-Electrode Configuration

Start from the Maxwell equation,

$$\nabla \cdot D = \rho \quad (3.3.1)$$

Dielectric displacement, or electric flux density, D , of pyroelectric is given by,

$$D = \epsilon_0 E + P_{pyro} \quad (3.3.2)$$

Pyroelectric polarization P_{pyro} consists of the initial polarization P_o (material specific), the polarization created by the induced electric field (related by dielectric susceptibility χ), and the polarization created by the temperature change,

$$P_{pyro} = P_o + \epsilon_0 \chi E + \lambda T \quad (3.3.3)$$

Pyroelectric coefficient λ is defined as,

$$\lambda \equiv \frac{dP}{dT} \quad (3.3.4)$$

In normal conditions, the heat received by the detector is small, and the resulting temperature change would be minimal. Therefore, it is safe to assume λ to be constant under small temperature excursions. Substitute P_{pyro} and λ back into Equation (3.3.1),

$$D = \varepsilon_0 E + \varepsilon_0 \chi E + P_o + \lambda T \quad (3.3.5)$$

In general, D , E , P , are rank tensors, but Section 3.2 established that they can be treated as one dimensional problems. Assume all charges flow out through the electrode and no surface charges left in the x direction,

$$\frac{\partial D}{\partial x} = \rho = 0 \quad (3.3.6)$$

$$\frac{\partial D}{\partial x} = 0 = \frac{\partial}{\partial x} \{ \varepsilon_0 E + \varepsilon_0 \chi E + P_o + \lambda T \} \quad (3.3.7)$$

$$0 = \varepsilon_0 \frac{\partial E}{\partial x} + \varepsilon_0 \chi \frac{\partial E}{\partial x} + \varepsilon_0 E \frac{\partial \chi}{\partial x} + \frac{\partial P_o}{\partial x} + \lambda \frac{\partial T}{\partial x} \quad (3.3.8)$$

Assume dielectric susceptibility χ does not vary with x ,

$$\varepsilon_0 E \frac{\partial \chi}{\partial x} = 0 \quad (3.3.9)$$

And the heat is not large enough to change the initial polarization P_o in the x direction,

$$\frac{\partial P_o}{\partial x} = 0 \quad (3.3.10)$$

Equation (3.3.8) reduces to,

$$\begin{aligned} \frac{\partial D}{\partial x} = 0 &= \varepsilon_0 \frac{\partial E}{\partial x} + \varepsilon_0 \chi \frac{\partial E}{\partial x} + \lambda \frac{\partial T}{\partial x} \\ 0 &= \varepsilon_0 (1 + \chi) \cdot \partial E + \lambda \cdot \partial T \end{aligned} \quad (3.3.11)$$

Integrate Equation (3.3.11),

$$0 = \varepsilon_0 (1 + \chi) \cdot \int_{E_1}^{E_2} \partial E + \lambda \cdot \int_{T_1}^{T_2} \partial T \quad (3.3.12)$$

$$0 = \varepsilon_0 (1 + \chi) \cdot (E_2 - E_1) + \lambda \cdot (T_2 - T_1)$$

Multiply by device parameter $x = a$,

$$0 = \varepsilon_0 (1 + \chi) \cdot (E_2 - E_1) \cdot a + \lambda \cdot (T_2 - T_1) \cdot a \quad (3.3.13)$$

$$-\varepsilon_0 (1 + \chi) \cdot (E_2 - E_1) \cdot a = \lambda \cdot (T_2 - T_1) \cdot a$$

Let

$$\Delta V = (E_2 - E_1) \cdot a \quad (3.3.14)$$

$$\Delta T = (T_2 - T_1)$$

Rearrange Equation (3.3.13) yields the relationship between the voltage and the temperature,

$$-\varepsilon_0 (1 + \chi) \cdot \Delta V = \lambda \cdot \Delta T \cdot a$$

$$\boxed{\Delta V = \frac{-\lambda \cdot a}{\varepsilon_0 (1 + \chi)} \cdot \Delta T} \quad (3.3.15)$$

To include time transient effects, let ΔT defined by Equation (3.2.1),

$$\boxed{\Delta V(t) = \frac{-\lambda \cdot a}{\varepsilon_0 (1 + \chi)} \cdot \Delta T(t)} \quad (3.3.16)$$

In summary, whenever the detector absorbs heat, any temperature change ΔT will create a voltage change ΔV . Electronic equipment can then be used to measure this voltage change.

3.4 Total Energy Laser Detector

The total energy of a laser pulse can be measured by the pyroelectric detector [6][7]. When a pyroelectric detector absorbs a radiation pulse, its surface temperature will rise and propagate into the body. The total induced charge has been shown to be independent of the spatial distribution of the incident energy [8]. If the pulse duration is less than the temperature rise propagation time from the surface to the rear, then the energy can only leave the detector

through radiation from the front surface. Because the detector's physical thermal conductance is greater than its radiative conductance, the energy loss will be negligible. Therefore, the measured charge is proportional to the pulse energy. The same principle can be applied to charge leakage. If the pulse duration is less than the detector's electrical RC time constant, then the charge leakage will also be negligible. This energy lossless assumption is only correct under certain conditions. At a distance $l_{1/e}$ below the surface, the time τ takes for the temperature to rise to $1/e$ of the surface's value is given by [4],

$$\tau = l_{1/e}^2 \frac{c'}{K} \quad (3.4.1)$$

where c' is volume specific heat, and K is thermal conductivity. If $l_{1/e}$ is the detector thickness size, the pulse duration must be much less than τ for the energy lossless assumption to hold. Likewise, if long pulse duration τ is desired, then the detector thickness must increase to accommodate. Base on the method outlined in Section 3.2, if the excess temperature at the surface is

$$T = T_o \cos \omega t \quad (3.4.2)$$

Solving for x , at a distance $l_{1/e}$ below surface where temperature amplitude reduces to $1/e$ of its surface value

$$l_{1/e} = \sqrt{\frac{2K}{\omega c'}} \quad (3.4.3)$$

Equation (3.4.1) and (3.4.3) together provide an approximation of the theoretical limit of the sample size and the radiation condition, where the energy lossless assumption is valid.

Density	Specific Heat	Volume Specific Heat	Thermal Conductivity
S	c	$c' = cS$	K
[gm / cm ³]	[$\frac{J}{gm K}$]	[$\frac{J}{cm^3 K}$]	[$\frac{W}{cm K}$]
4.644	0.628	2.916	0.056

Table 3.4-1 Lithium Niobate $LiNbO_3$ thermal properties at 300K^[9].

Consider a detector with thickness $l = 0.5\text{mm}$, that has properties from Table 3.4-1, and the light source frequency is $\omega = 2\pi f$; use the sample thickness as $l_{1/e}$ to obtain the maximum allowed pulse duration τ from Equation (3.4.1), and $l_{1/e}$ can be calculated from Equation (3.4.3). Their results are listed in Table 3.4-2.

Light Source	Wavelength	Frequency f	$l_{1/e}$	τ
	[μm]	[Hz]	[cm]	[sec]
N ₂ Laser	0.303	9.90×10^{14}	2.48×10^{-9}	0.13
Modulated				
Diode Laser	0.85	3.53×10^{14}	4.16×10^{-9}	0.13

Table 3.4-2 Calculated limits of the detector size and the light exposure time.

Hence, if Lithium Niobate is used to measure the prospective N₂ laser or the modulated Diode laser, then the detector thickness should be greater than the respective calculated $l_{1/e}$ and the

pulse exposure time should be less than τ . In this work, all samples' thicknesses a are much greater than $l_{1/e}$, and their exposure times are less than τ . It shall be noted that even at the highest $l_{1/e}$ value of 4.16×10^{-9} cm, it only represents 8.32×10^{-8} of the total detector thickness. Therefore, it is safe to assume that most of the heat conduction occurs on the surface, which meets the assumption criteria of the total energy detector. The thermal properties listed in Table 3.4-1 are functions of the temperature. All previously mentioned calculations are thus only valid at 300K, which was the temperature that this experiment conducted at. From the model currently presented, there are possible schemes to speed up the detector performance. By further inspection of Equation (3.4.1), it may be feasible to reduce the detector signal response time by decreasing $l_{1/e}$, perhaps achievable through the application of a more efficient light/heat absorbing layer on the detector surface.

CHAPTER 4 SAMPLES AND EXPERIMENT

Figure 4.1-1 shows the experiment schematic set up. The detector sample in the Edge-Electrode configuration was mounted in front of a laser source. The electrode is chromium metal evaporated onto LiNbO₃ wafer before the wafer was cut into various sample sizes. A BNC connector with soldered aluminum wire in contact with top and bottom electrodes holds the sample in place. This BNC connector connects to an amplifier. HP 57111a Digitizing Oscilloscope connects the amplifier for the signal voltage readout. BNC, the connecting wires, the amplifier, the oscilloscope, all have 50Ω impedance and are verified by HP 8702B Lightwave Component Analyzer across spectrum of 300KHz to 3GHz. N₂ laser with 0.303 μm center wavelength and modulated diode laser with 0.85 μm center wavelength were used as light sources. During sample measurements, all external lightings were off except the light source. The detector was housed in an aluminum cylindrical enclosure with one opening pointing at the light source. The primary function of the aluminum cage was to isolate the detector from the ambient light and other electromagnetic interferences.

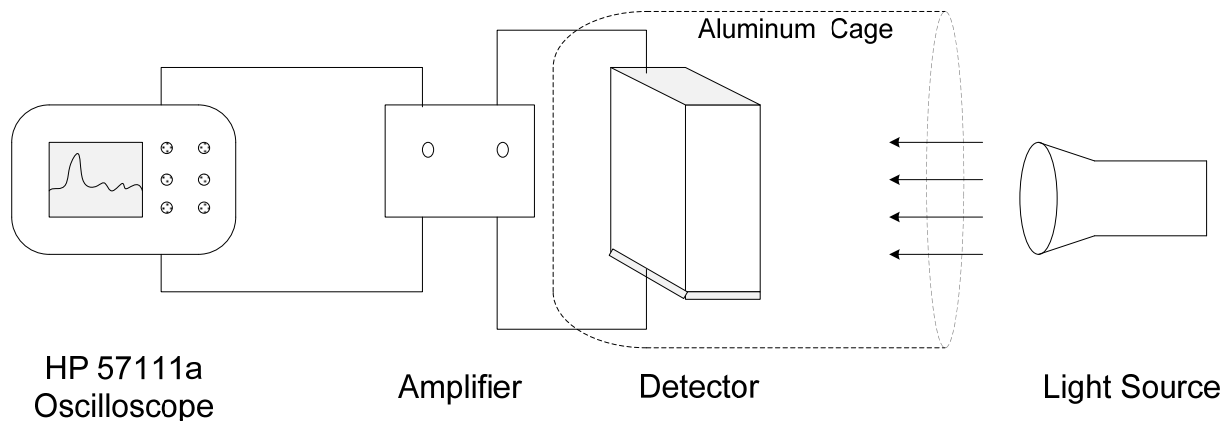


Figure 4.1- 1 Experiment Schematic Set Up

CHAPTER 5 RESULTS AND DISCUSSION

LiNbO₃ samples were successfully cut at the correct crystal orientation that suppressed the ringing effect. To illustrate the ringing effect impact, two samples shown in Figure 5-1 have different crystal orientations, but have identical physical dimensions of 0.5 mm x 1 mm x 1 mm. In Figure 5.0-1, the ringing-not-suppressed sample shows a high oscillating signal decay behavior that renders the detector useless in high frequency operation, whereas the ringing-suppressed sample shows a clean single spike response. This signal decay difference proves the existence of a LiNbO₃ crystal orientation, that suppresses (or decouples) inherent mechanical stress and strain in piezoelectric.

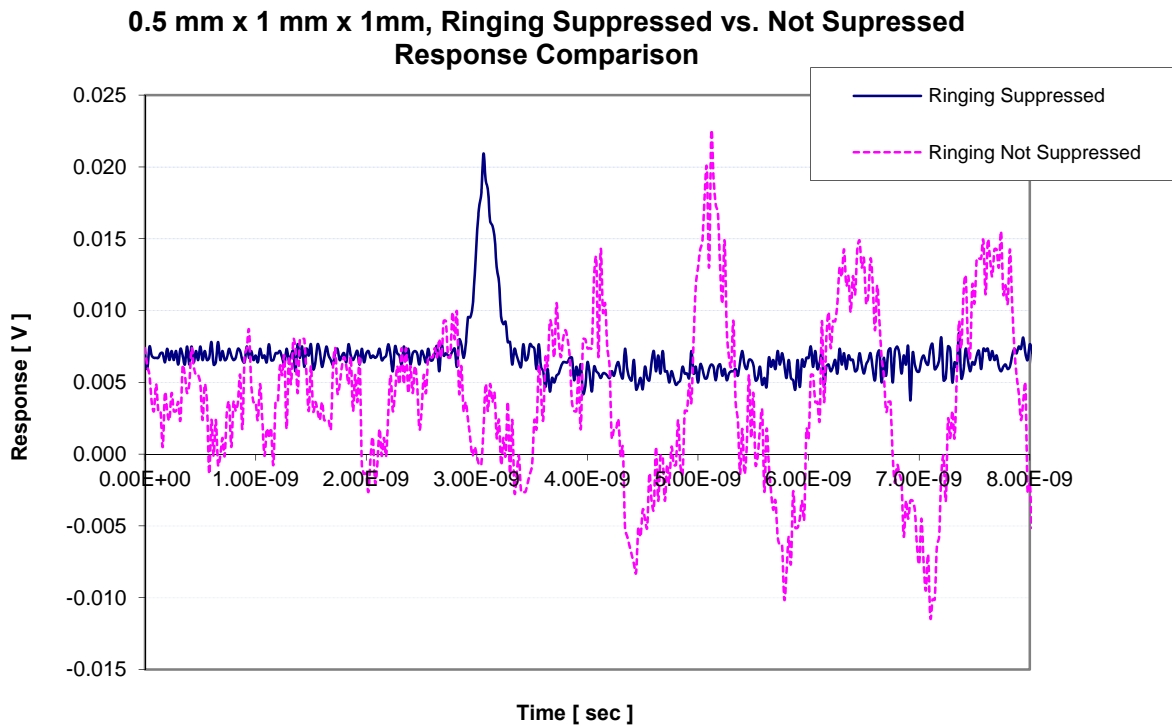


Figure 5.0 - 1 Signal response between ringing suppressed and not-suppressed samples

5.1 Not-Coated Samples under N₂ Laser Exposure

Subsequent samples were all cut at the ringing suppressed crystal orientation with varying thicknesses a . The samples cross sectional areas $b \times c$ were kept fixed at 1mm x 1mm. The illuminated surfaces were not coated with any light absorbing layer. In order to verify ringing suppression across all three dimensions, side exposure (irradiated area is $a \times c$) response data were also taken. The measured response data in Figures 5.1-1 to 6 all demonstrated ringing suppressions. The obtained full range response times for the not-coated samples have range from 3.40×10^{-10} to 6.80×10^{-10} seconds. Table 5-1 summarizes the measured signal response time of these samples. The signal rise time is the time that the sample takes to go from 10% to 90% of the maximum signal voltage, and vice versa for the fall time. The signal voltage reference zero was set at the second highest measured peak response voltage. A direct response time comparison of the frontal and side exposure is shown in Figure 5.1-7. The little difference in response time between the frontal and side exposure from Figure 5.1-7 suggests that heat dissipation was sufficiently fast, and thus required no additional background cooling. In addition, the ability to obtain electrical signal from light exposure proves that the heat transfer and charge models remain valid under ringing reduction.

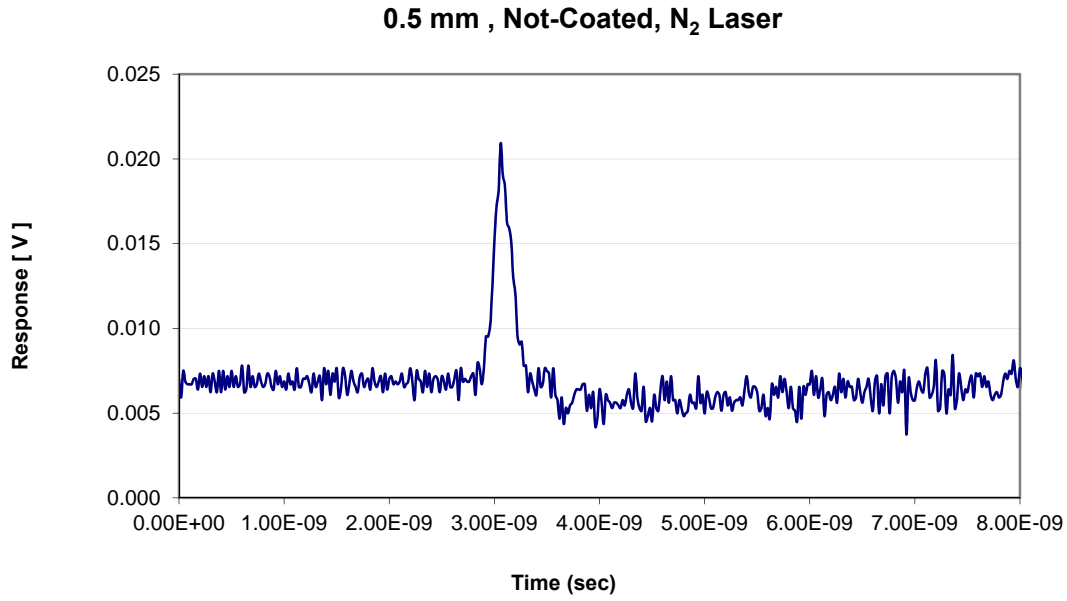


Figure 5.1- 1 Not-coated, 0.5 mm thick, N₂ laser frontal exposure response.

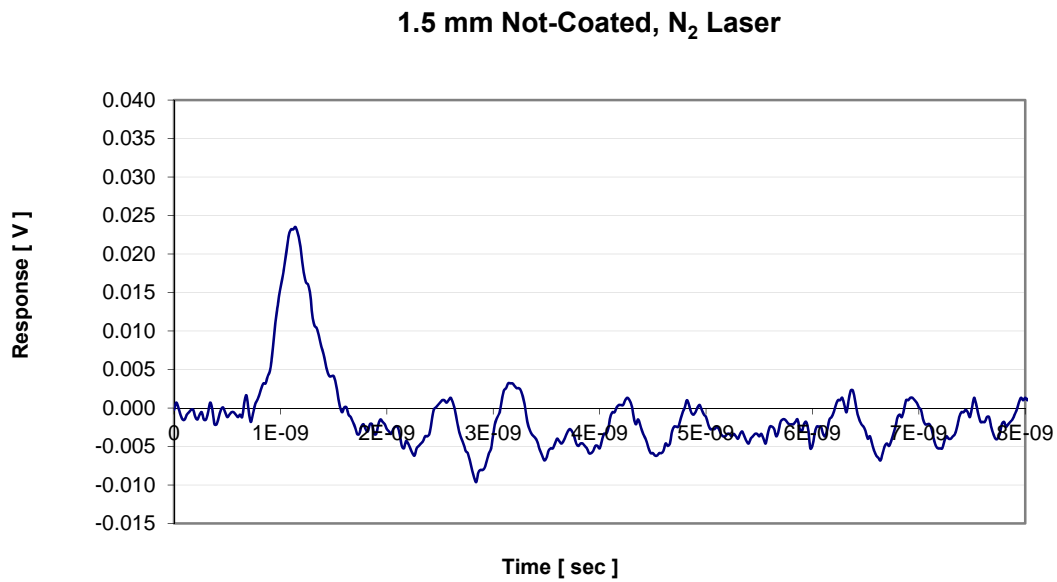


Figure 5.1- 2 Not-coated, 1.5 mm thick, N₂ laser frontal exposure response.

2.5 mm Not-Coated, N₂ Laser

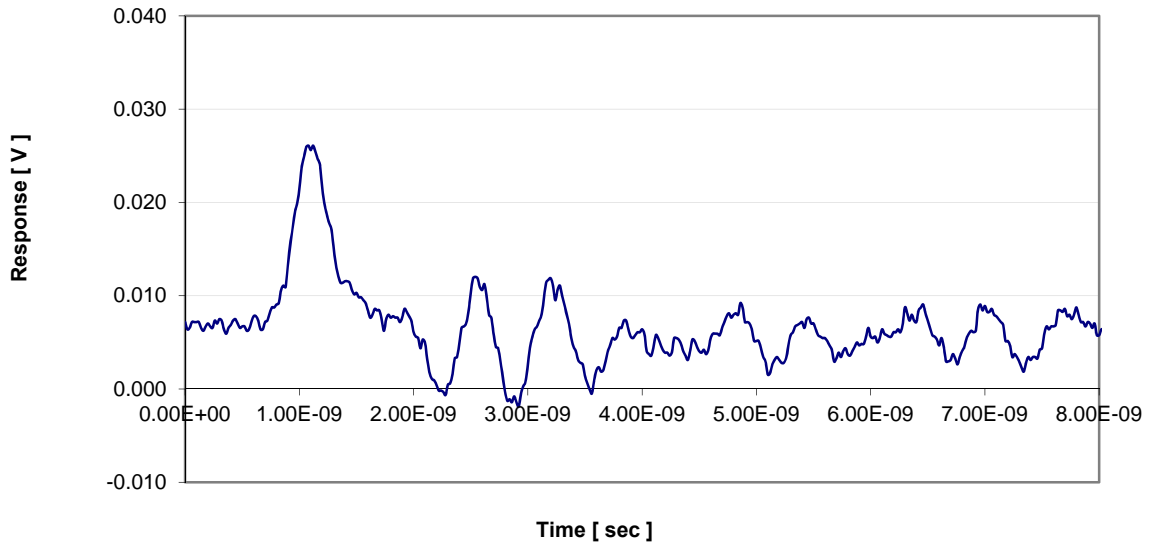


Figure 5.1- 3 Not-coated, 2.5 mm thick, N₂ laser frontal exposure response.

4.0 mm Not-Coated, N₂ Laser

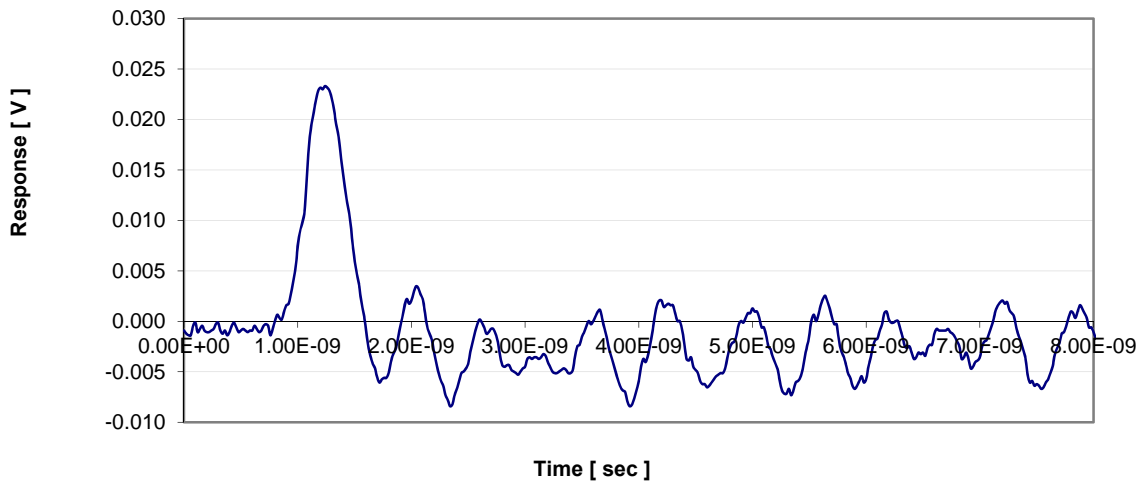


Figure 5.1- 4 Not-coated, 4.0 mm thick, N₂ laser frontal exposure response.

1.5 mm Side Exposure, Not-Coated, N₂ Laser

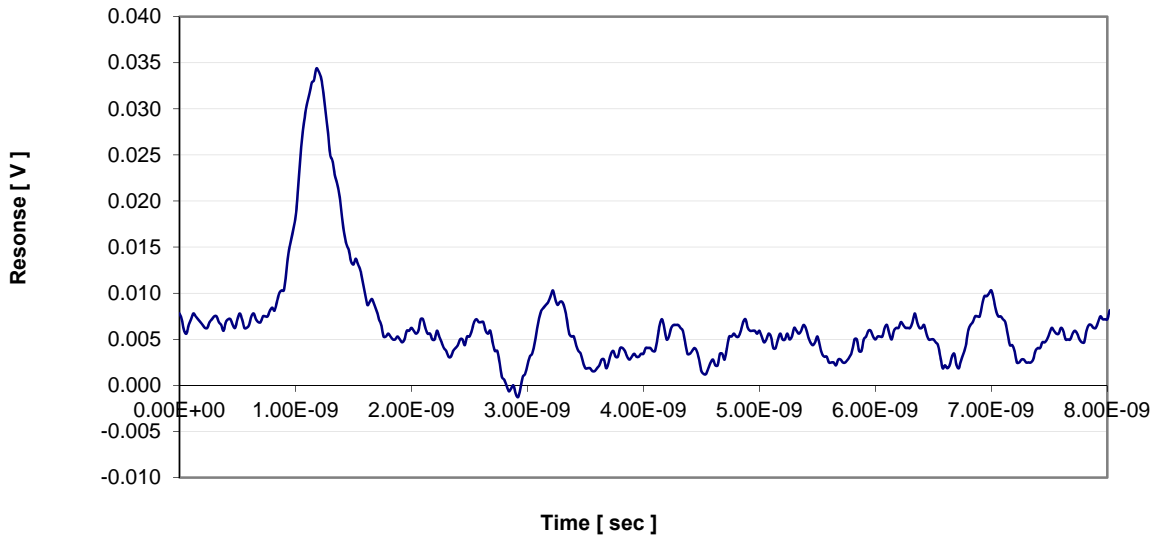


Figure 5.1- 5 Not-coated, 1.5 mm thick, N₂ laser side exposure response.

2.5 mm Side Exposure, Not-Coated, N₂ Laser

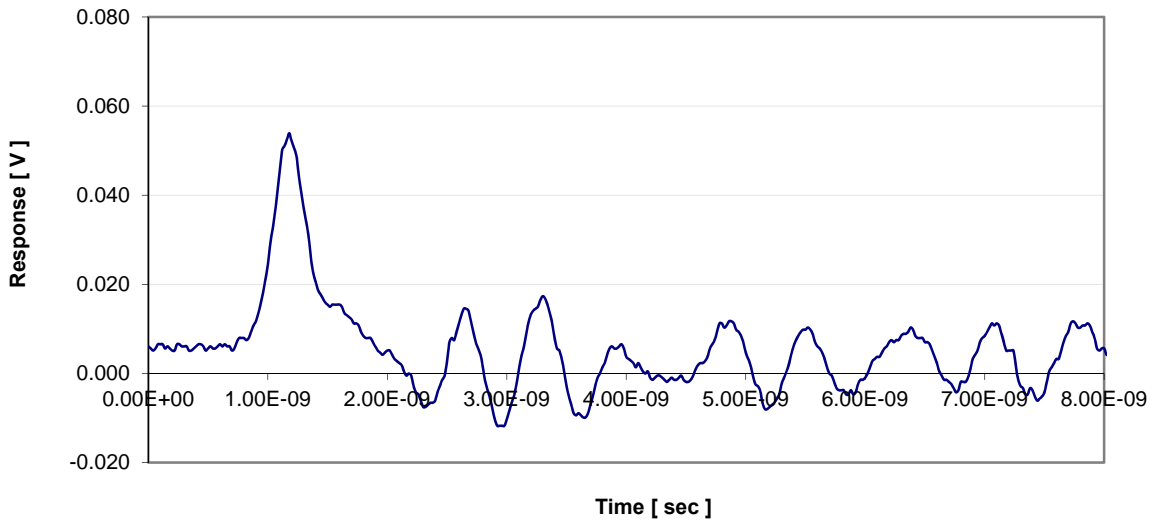


Figure 5.1- 6 Not-coated, 2.5 mm thick, N₂ laser side exposure response.

Frontal Exposure	Thickness <i>a</i> [mm]	Rise Time (10% to 90 %) [sec]	Fall Time (90% to 10%) [sec]	Rise + Fall Full Range Time (10% to 10%) [sec]
	0.5	1.40×10^{-10}	2.00×10^{-10}	3.40×10^{-10}
	1.5	2.40×10^{-10}	3.20×10^{-10}	5.60×10^{-10}
	2.5	2.80×10^{-10}	4.00×10^{-10}	6.80×10^{-10}
	4	2.20×10^{-10}	2.40×10^{-10}	4.60×10^{-10}
Side Exposure				
	1.5	2.00×10^{-10}	3.20×10^{-10}	5.20×10^{-10}
	2.5	2.00×10^{-10}	4.50×10^{-10}	6.50×10^{-10}

Table 5.1- 1 Response time summary for the not-coated samples under N₂ laser exposure.

Side, Frontal Exposure Rise + Fall Full Range Time Comparison, N₂ Laser

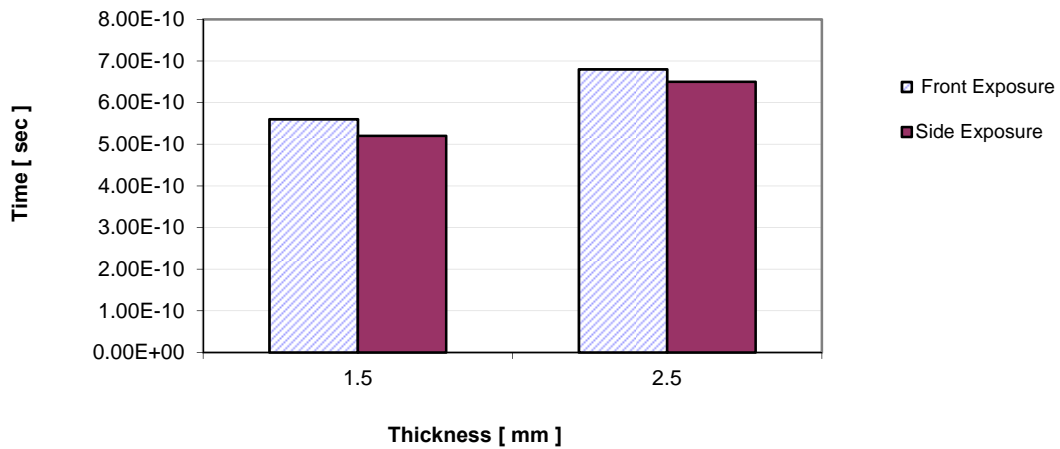


Figure 5.1- 7 Full response time comparison between the frontal and the side exposure under N₂ laser.

5.2 Black Coated Samples under N₂ Laser Exposure

In order to observe probable performance enhancements, a black absorbing layer (Nextel black velvet coating, manufacturer reported emissivity $e = 0.97$) was painted on the irradiated area $b \times c$. The measured response data in Figure 5.2-1 ~ 4 show that ringing suppression remains effective with the added black coat. These black-coated samples' response times range from 2.60×10^{-10} to 7.00×10^{-10} seconds, and are summarized in Table 5.2-1. When the response times between the not-coated and the black-coated samples were compared in Figure 5.2-5, the black-coated samples response times occasionally were shorter, but sometimes they were longer. Therefore, there are no clear indications that a black absorbing layer will always provide a faster response.

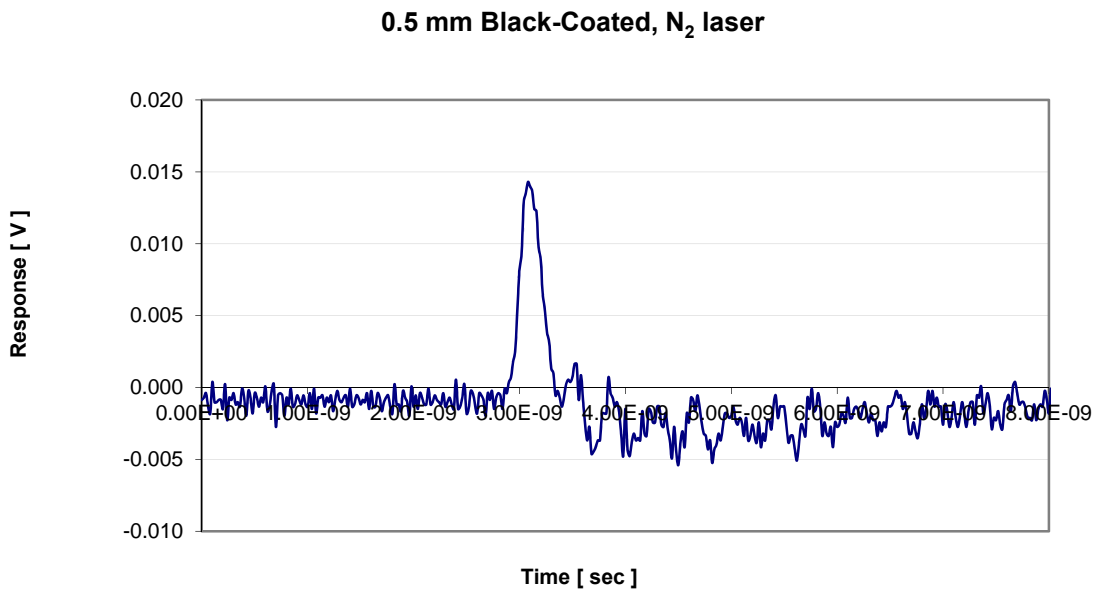


Figure 5.2- 1 Black-coated, 0.5 mm thick, N₂ laser frontal exposure response.

1.5 mm Black-Coated, N₂ Laser

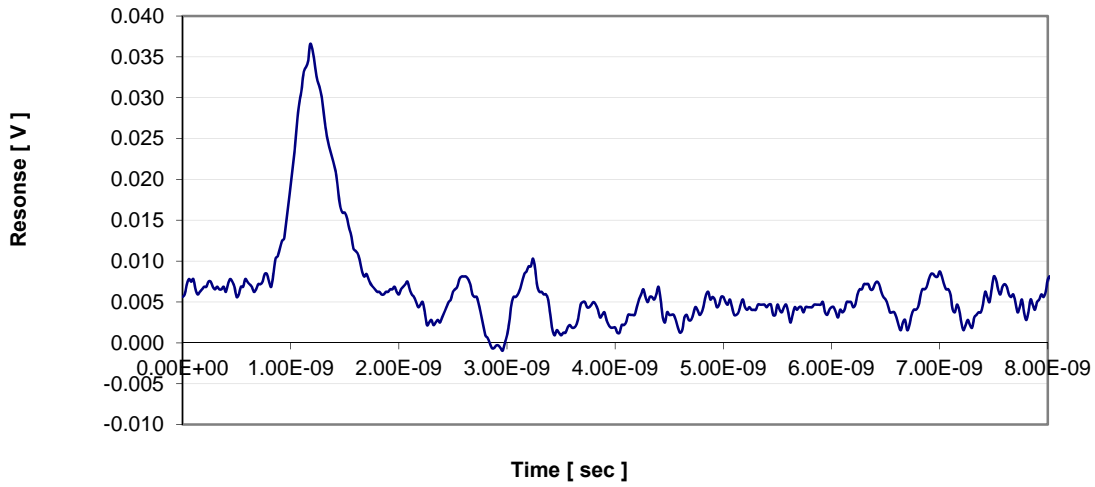


Figure 5.2- 2 Black-coated, 1.5 mm thick, N₂ laser frontal exposure response.

2.5 mm Black-Coated, N₂ Laser

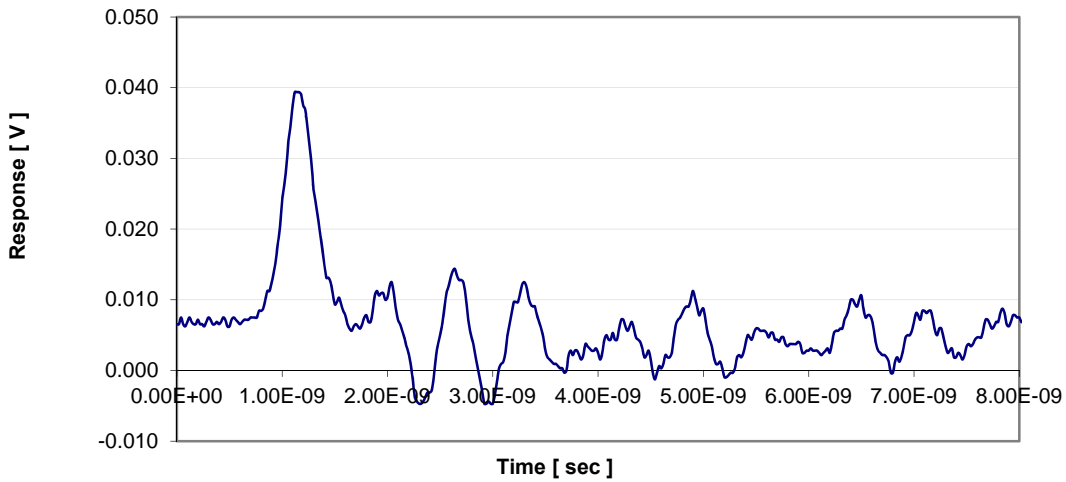


Figure 5.2- 3 Black-coated, 2.5 mm thick, N₂ laser frontal exposure response.

4.0 mm Black-Coated, N₂ Laser

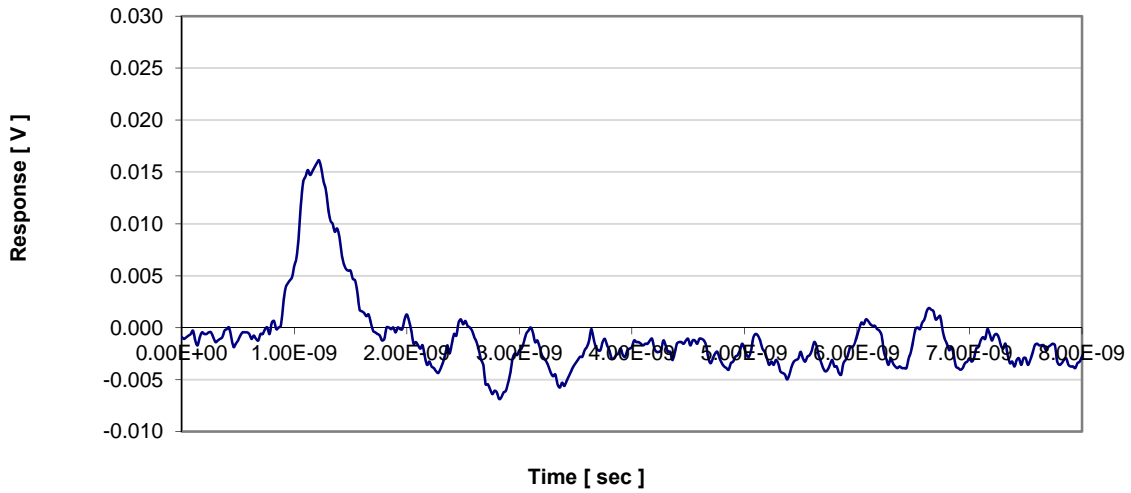


Figure 5.2- 4 Black-coated, 4.0 mm thick, N₂ laser frontal exposure response.

Black-Coated Vs. Not-Coated Total Time Comparison N₂ Laser

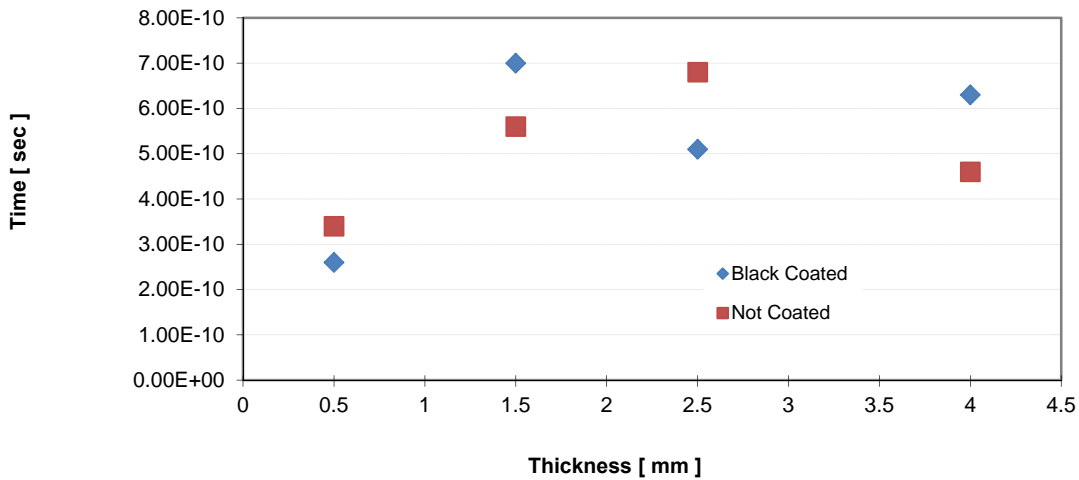


Figure 5.2- 5 Full response time comparison between Black-coated and Not-Coated samples under N₂ laser exposure .

Thickness <i>a</i> [mm]	Rise Time (10% to 90 %) [sec]	Fall Time (90% to 10%) [sec]	Rise + Fall Full Range Time (10% to 10%) [sec]
0.5	1.00×10^{-10}	1.60×10^{-10}	2.60×10^{-10}
1.5	3.00×10^{-10}	4.00×10^{-10}	7.00×10^{-10}
2.5	2.50×10^{-10}	2.60×10^{-10}	5.10×10^{-10}
4	2.10×10^{-10}	4.20×10^{-10}	6.30×10^{-10}

Table 5.2-1 Response time summary for the black-coated samples under N₂ laser exposure.

5.3 Modulated Diode Laser as the Light Source

For verification purposes, the experiment was repeated on the same samples but with modulated diode laser as the light source. The response data are shown in Figure 5.3-1 to Figure 5.3-4. All samples demonstrated successful ringing suppression and their response times are summarized in Table 5.3-1. The fastest full range response time obtained was 3.80×10^{-10} sec, and the longest time was 6.20×10^{-10} sec; both were much less than the calculated theoretical exposure time limit. When the response times of the not-coated and the black-coated samples were compared in Figure 5.3-7, both samples' data showed shorter response time as thickness decreased. However, the black-coated sample produced longer response time instead of the expected speed enhancement.

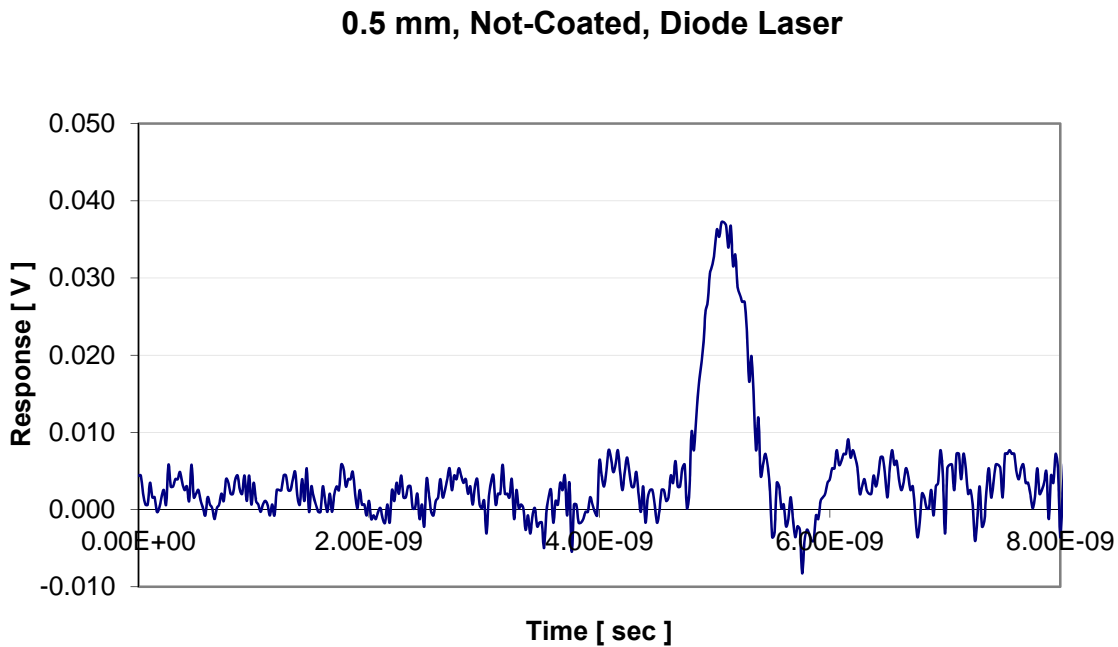


Figure 5.3 - 1 Not-coated, 0.5 mm thick, Diode laser frontal exposure response.

1.5 mm, Not-Coated, Diode Laser

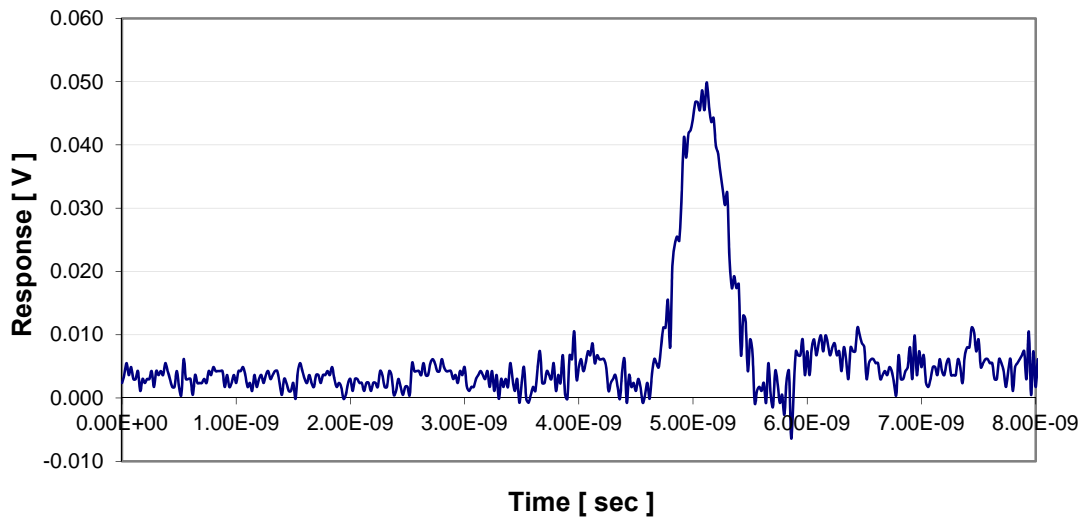


Figure 5.3 - 2 Not-coated, 1.5 mm thick, diode laser frontal exposure response.

2.5 mm , Not-Coated, Diode Laser

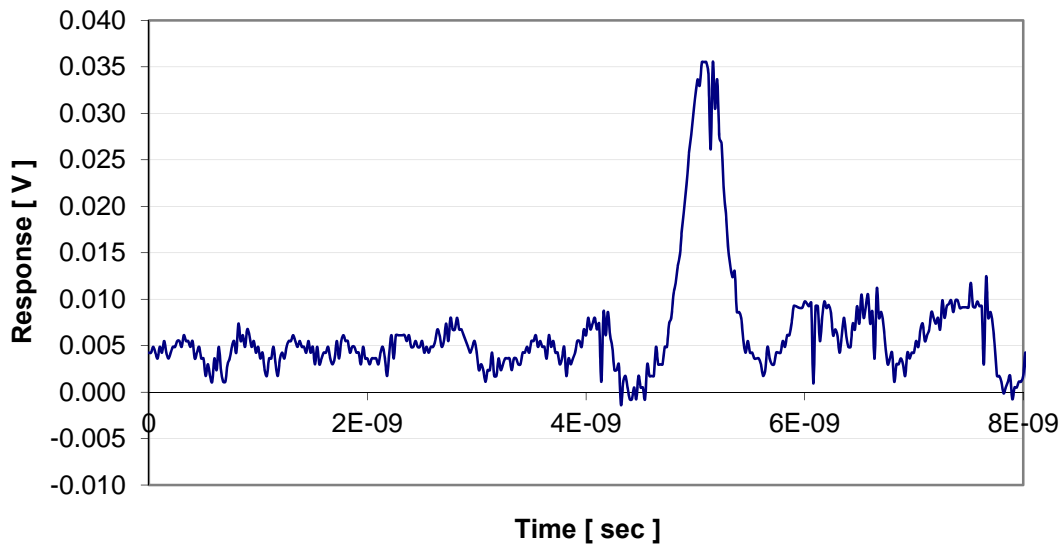


Figure 5.3 - 3 Not-coated, 2.5mm thick, diode laser frontal exposure response.

4.0 mm, Not-Coated, Diode Laser

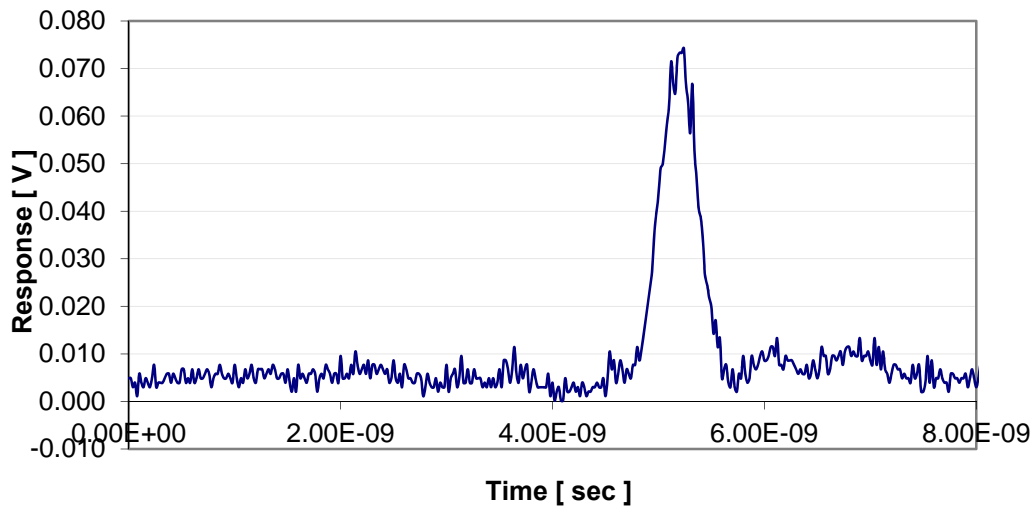


Figure 5.3 - 4 Not-coated, 4.0 mm thick, diode laser frontal exposure response.

2.5 mm, Black-Coated, Diode Laser

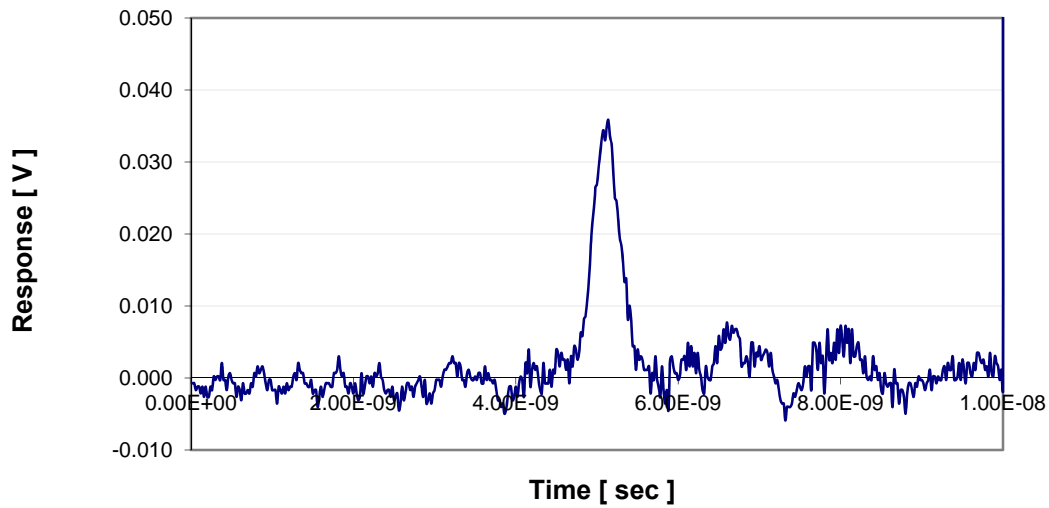


Figure 5.3 – 5 Black-coated, 2.5mm thick, diode laser frontal exposure response.

4.0 mm, Black-Coated, Diode Laser

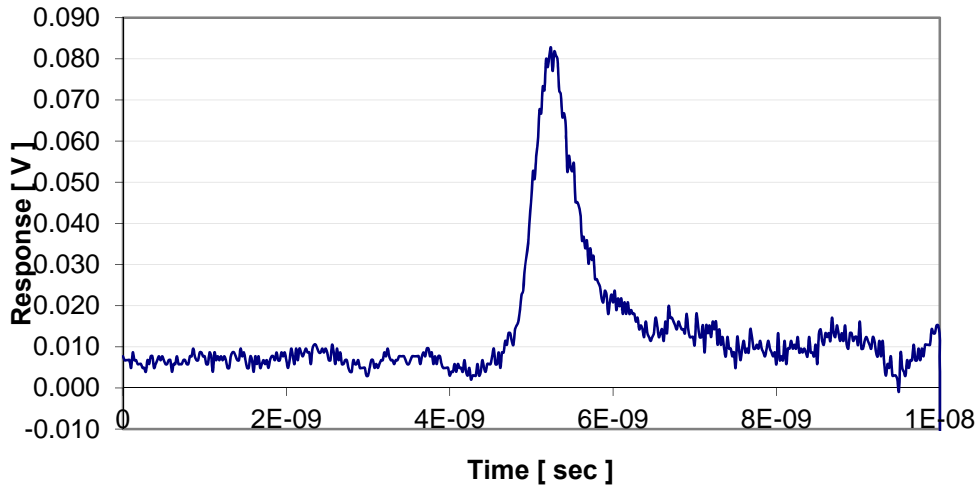


Figure 5.3 – 6 Black-coated, 4mm thick, diode laser frontal exposure response.

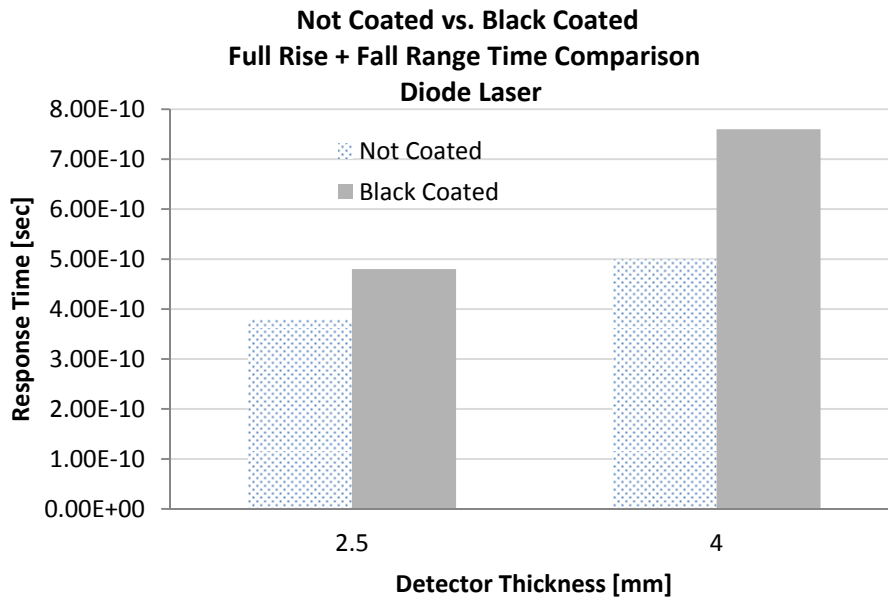


Figure 5.3 – 7 Not-coated and black-coated sample response time comparison under diode laser exposure.

Not-Coated	Thickness <i>a</i> [mm]	Rise Time (10% to 90 %) [sec]	Fall Time (90% to 10%) [sec]	Rise + Fall Full Range Time (10% to 10%) [sec]
Frontal Exposure	0.5	2.20×10^{-10}	3.00×10^{-10}	5.20×10^{-10}
	1.5	2.80×10^{-10}	3.40×10^{-10}	6.20×10^{-10}
	2.5	1.80×10^{-10}	2.00×10^{-10}	3.80×10^{-10}
	4	2.40×10^{-10}	2.60×10^{-10}	5.00×10^{-10}
Black-coated	2.5	2.30×10^{-10}	2.50×10^{-10}	4.80×10^{-10}
Frontal Exposure	4	2.60×10^{-10}	5.00×10^{-10}	7.60×10^{-10}

Table 5.2-1 The response time summary for samples under diode laser exposure.

CHAPTER 6 SUMMARY AND CONCLUSION

The acquisition of non-oscillating data proves the existence of a crystal orientation that will suppress the ringing effect inside LiNbO_3 , and most importantly, the heat transfer and charge models remained valid with different crystal orientation cuts. The attained response range times for the ringing-reduced, not-coated samples are from 0.34 ns to 0.68 ns. The measured response range times for the black-coated samples are from 0.26 ns to 0.76 ns. By comparing the response time of the not-coated and the black-coated samples, the comparison shows that the added black absorbing layer does not guarantee device speed enhancement when the sample thickness is much greater than $l_{1/e}$. By irradiating the same sample on the side instead of the front, the data proves that not only the crystal angle is good for suppressing ringing across all three dimensions, but also that heat dissipation within the sample is fast enough so that no additional external cooling is needed. Depending on circumstances, samples exhibit a general trend of reducing response time with decreasing thickness, which matches the model prediction presented in this work.

Appendix A – Temperature Profile When $T_{back} \neq 0$

This appendix shows how to obtain temperature profile when back ground temperature T_{back} is not set to zero.

General set up is same as Figure 3.2-1, except $T_{back} \neq 0$, which is repeated here as Figure A-1 for convenience.

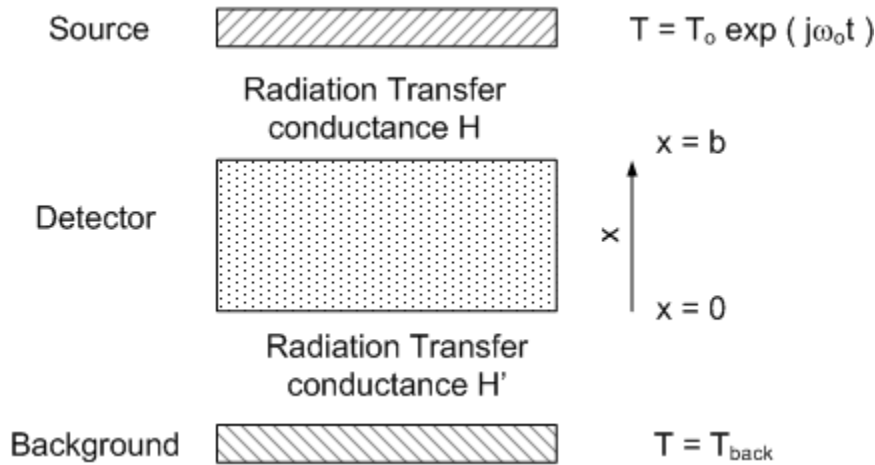


Figure A- 1 Single layer pyroelectric detector with radiation from back surface.

Start from general solution,

$$T(x) = A \cosh(\omega x) + B \sinh(\omega x) \quad (\text{A.1})$$

$$\frac{\partial T}{\partial x} = A \omega \sinh(\omega x) + \omega B \cosh(\omega x) \quad (\text{A.2})$$

Apply boundary conditions and solve for constants A and B:

$$\text{At } x = 0 : \quad K \frac{\partial T}{\partial x} = H (T - T_{back}) \quad (\text{A.3})$$

$$\left. \frac{dT}{dx} \right|_{x=0} = \omega B \quad (\text{A.4})$$

$$T(x=0) = A \quad (\text{A.5})$$

$$K\omega B = H'(A - T_{back}) \quad (\text{A.6})$$

$$B = \frac{H'}{K\omega}(A - T_{back}) \quad (\text{A.7})$$

$$\text{At } x = b: \quad K \frac{\partial T}{\partial x} = H(T_o - T) \quad (\text{A.8})$$

$$K\omega \{A \sinh(\omega b) + B \cosh(\omega b)\} = H \{T_o - A \cosh(\omega b) - B \sinh(\omega b)\} \quad (\text{A.9})$$

$$K\omega \left\{ A \sinh(\omega b) + \frac{H'}{K\omega}(A - T_{back}) \cosh(\omega b) \right\} = H \left\{ T_o - A \cosh(\omega b) - \frac{H'}{K\omega}(A - T_{back}) \sinh(\omega b) \right\}$$

$$A = \frac{T_o + T_{back} \left[\left(\frac{H'}{K\omega} \right) \sinh(\omega b) + \frac{H'}{H} \cosh(\omega b) \right]}{\left[\left(\frac{K\omega}{H} \right) + \left(\frac{H'}{K\omega} \right) \right] \sinh(\omega b) + \left[\frac{H'}{H} + 1 \right] \cosh(\omega b)} \quad (\text{A.11})$$

Substitute A and B back into $T(x)$,

$$T(x) = A \cosh(\omega x) + B \sinh(\omega x) \quad (\text{A.12})$$

$$T(x) = A \cosh(\omega x) + \frac{H'}{K\omega}(A - T_{back}) \sinh(\omega x) \quad (\text{A.13})$$

$$T(x) = \left\{ \cosh(\omega x) + \frac{H'}{K\omega} \sinh(\omega x) \right\} A - \frac{H'}{K\omega} T_{back} \sinh(\omega x) \quad (\text{A.14})$$

Appendix B – Temperature Only Varies With Distance x

This appendix shows the derivation of θ_0 in Equation (3.2.3).

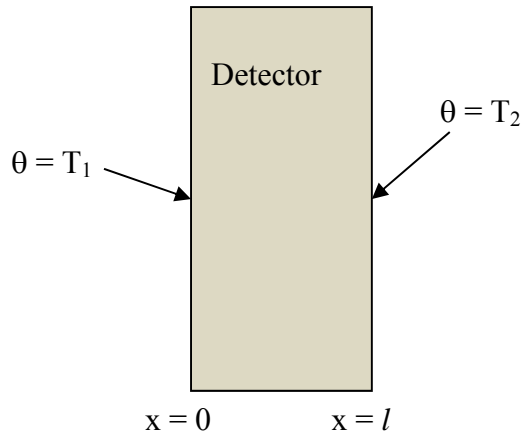


Figure B - 1 Temperature that only varies in x in a detector

The one dimensional heat flow equation is

$$\frac{\partial \theta}{\partial t} = k \frac{\partial^2 \theta}{\partial x^2} \quad \text{where } \theta \text{ is temperature} \quad (\text{B.1})$$

Because the temperature θ is a function of the distance x only

$$\frac{\partial \theta}{\partial t} = 0 \quad \text{Hence,} \quad \frac{\partial^2 \theta}{\partial x^2} = 0 \quad (\text{B.2})$$

Integrate Equation (B.2) yields

$$\frac{d\theta}{dx} = a \quad (\text{B.3})$$

Integrate again on Equation (B.3)

$$\theta = ax + b \quad (\text{B.4})$$

Boundary conditions are $\theta = T_1$ at $x = 0$, $\theta = T_2$ at $x = l$

$$\theta(0) = T_1 = a(0) + b = b \quad (\text{B.5})$$

$$\theta(l) = T_2 = a(l) + T_1 \rightarrow a = \frac{T_2 - T_1}{l} \quad (\text{B.6})$$

Therefore,

$$\theta(x) = \frac{T_2 - T_1}{l} x + T_1 \quad (\text{B.7})$$

That is θ_0 in Equation (3.2.3).

References

1. L. Capineri, et al., *IEEE Sensors Journal*, vol.5, no.3, Jun 2005
2. Sze, *Physics of Semiconductor Devices*, 1981
3. Tang, *Ringling Effects in High Speed Pyroelectric Detectors Using Lithium Niobate*, MS Thesis, UCLA, 1999
4. Putley, E.H, *Semiconductors and Semimetals*, Volume 5, p 259-285, 1970
5. Holeman B.R. *Infrared Physics*, Vol. 12, p 125-135, 1972
6. M.Shimazu, Y.Suzaki, et al., *Japan J. Appl. Phys*, Vol. 6, p120, 1967
7. R.W. Astheimer, R.E. Buckley, *Rev.Sci.Instr*, Vol.38, p 1764 -1768, 1967
8. J. Cooper, *J.Sci. Inst.*, Vol.39, p 467-472, 1962
9. V.V.Zhdanova, V.P.Klyuev, V.V.Lemanov, I.A.Smirnov, and V.V.Tikhonov, *Sov.Phys.- Solid State (USA)* **10**,(6) 1360 (1968).